

## Seasonal and Latitudinal Variability of the Gravity Wave Spectrum in the Lower Stratosphere

Erik A. Lindgren<sup>1,2</sup> , Aditi Sheshadri<sup>2</sup> , Aurélien Podglajen<sup>3</sup> , and Robert W. Carver<sup>4</sup>

<sup>1</sup>Swiss Re, Armonk, NY, USA, <sup>2</sup>Department of Earth System Science, Stanford University, Stanford, CA, USA,

<sup>3</sup>Laboratoire de Météorologie Dynamique, UMR 8539, CNRS/PSL-ENS/Sorbonne Université/Ecole Polytechnique, Paris, France, <sup>4</sup>Loon LLC, Mountain View, CA, USA

### Key Points:

- Loon LLC superpressure balloons can be used to infer lower stratospheric gravity wave (GW) motions over most latitudes and all seasons
- Seasonal and latitudinal variability is found in GW spectral slopes and amplitudes over the full intrinsic frequency spectrum
- GW amplitudes are higher during positive QBO phases compared to negative phases for intrinsic frequencies up to the buoyancy frequency

### Supporting Information:

- Supporting Information S1

### Correspondence to:

E. A. Lindgren,  
erikanderslindgren@gmail.com

### Citation:

Lindgren, E. A., Sheshadri, A., Podglajen, A., & Carver, R. W. (2020). Seasonal and latitudinal variability of the gravity wave spectrum in the lower stratosphere. *Journal of Geophysical Research: Atmospheres*, 125, e2020JD032850. <https://doi.org/10.1029/2020JD032850>

Received 31 MAR 2020

Accepted 27 AUG 2020

Accepted article online 30 AUG 2020

**Abstract** Superpressure balloon data of unprecedented coverage from Loon LLC is used to investigate the seasonal and latitudinal variability of lower stratospheric gravity waves over the entire intrinsic frequency spectrum. We show that seasonal variability in both gravity wave amplitudes and spectral slopes exist for a wide range of intrinsic frequencies and provide estimates of spectral slopes in five latitudinal regions for all four seasons, in five different frequency windows. The spectral slopes can be used to infer gravity wave amplitudes of intrinsic frequencies as high as 70 cycles/day from gravity waves resolved in model and reanalysis data. We also show that a robust relationship between the phase of the quasi-biennial oscillation and gravity wave amplitudes exists for intrinsic frequencies as high as the buoyancy frequency. These are the first estimates of seasonal and latitudinal variability of gravity wave spectral slopes and high-frequency amplitudes and constitute a significant step toward obtaining observationally constrained gravity wave parameterizations in climate models.

## 1. Introduction

Gravity waves (GWs) play a substantial role in controlling the stratospheric and tropospheric circulations. They play a leading order role in driving the middle atmosphere circulation (Fritts & Alexander, 2003) and have a large influence on its variability in both tropical (Baldwin et al., 2001) and polar regions (e.g., de la Cámara et al., 2016). They are responsible for ubiquitous temperature fluctuations (Gary, 2006) which impact the formation (Dinh et al., 2016; Jensen et al., 2016; Spichtinger & Krämer, 2013) and evolution (Podglajen et al., 2018) of upper-tropospheric cirrus clouds, as well as polar stratospheric cloud formation (Alexander et al., 2013; Hoffmann et al., 2017). Finally, their breaking generates turbulence which contributes to tracer transport (Pavelin et al., 2002; Podglajen et al., 2017).

Although important for atmospheric dynamics and circulation, GWs on scales of  $10^2$ – $10^5$  m and periods shorter than an hour are typically not available in data from conventional observational systems such as satellites nor properly resolved in atmospheric models (e.g., Alexander et al., 2010). In models, these waves must therefore be estimated, or parameterized, from the resolved flow. Current state-of-the-art parameterizations are severely limited by computational necessity and the scarcity of observations. Uncertainties in GW momentum transport limit our ability to predict the response of the tropospheric and stratospheric circulation to global warming (e.g., Karpechko & Manzini, 2012; Polichtchouk et al., 2018; Sigmond & Scinocca, 2010; van Niekerk et al., 2018). They also impact subseasonal-to-seasonal forecasts (e.g., Alexander et al., 2019). Available observations are limited by different observational filters and are generally insufficient to constrain GW momentum fluxes; estimates of GW drag are uncertain by a factor of 10 or more (Geller et al., 2013). Hence, there is a great need for new observational constraints on the GW field.

Superpressure balloons (SPBs) provide a unique way to characterize the entire GW spectrum and its variability. SPBs fly in the lower stratosphere where they are advected by the winds, and measurements of the SPBs are therefore done in the frame of reference of disturbances (i.e., the SPBs measure the intrinsic frequency of perturbations). SPBs have been used to measure GW activity in the Arctic (Hertzog et al., 2002; Pommereau et al., 2002), Antarctic (Hertzog et al., 2007, 2008; McDonald & Hertzog, 2008; Rabier et al., 2013), and tropical (Podglajen et al., 2016; Pommereau et al., 2011) regions; assess the accuracy of reanalyses in the lower stratosphere (e.g., Boccara et al., 2008; Friedrich et al., 2017; Podglajen et al., 2014); measure vertical wind and temperature fluctuations in the lower stratosphere associated with

GWs (Podglajen et al., 2016; Schoeberl et al., 2017); assess the representation of the GW spectrum in (re)analyses (Podglajen et al., 2020); improve data assimilation systems (Coy et al., 2019; Dharmalingam et al., 2019); and investigate the inertial peak in stratospheric wind and horizontal kinetic energy spectra in the Southern Hemisphere (SH) (Conway et al., 2019).

Although they have proven invaluable for the study of GW activity, scientific SPB data sets have traditionally been limited in their spatial and seasonal coverage, with flights typically restricted to a given season and latitude band. For example, Podglajen et al. (2016) used three SPB flights in the tropical pipe (from February to May) and 19 SPB flights in the decaying southern polar vortex (from September to January) in their analysis. In contrast, Loon LLC (previously Project Loon; hereafter Loon) has been continuously launching SPBs into the lower stratosphere since 2013 in their effort to provide worldwide Internet coverage, thus sampling all seasons and latitudes outside of the polar regions. More than 1,000 Loon SPB flights are currently available for analysis. Unlike previous SPB data sets, the Loon measurements were not designed for scientific use, and they require dedicated processing to overcome missing data or vertical maneuvers, which might result in artifacts, in particular at the highest GW frequencies (Conway et al., 2019). Keeping this limitation in mind, the unprecedented temporal and spatial SPB coverage still provides a wealth of new information on the GW field. Four of the above mentioned studies (Conway et al., 2019; Coy et al., 2019; Friedrich et al., 2017; Schoeberl et al., 2017) made use of Loon data in their analysis; two of them investigated characteristics of GWs (Conway et al., 2019; Schoeberl et al., 2017).

Spectral slopes of GW disturbances have been shown to obey a power law of format  $\hat{\omega}^\gamma$ , where  $\hat{\omega}$  is intrinsic frequency and  $\gamma$  is a constant. This is generally true between frequencies from the inertial frequency (Coriolis frequency) up to more than 100 cycles/day. For comparison, the Coriolis frequency ranges from 0.5 to 1.5 cycles/day from latitudes of 90° to 20°, while the buoyancy frequency in the lower stratosphere ( $N$ ) is generally around 300 cycles/day. Estimates of  $\gamma$  in this frequency range are typically close to  $-2$ , and the GW power law dependence is thought to be the result of a saturated energy cascade (e.g., Bacmeister et al., 1996; Dewan, 1994; Smith et al., 1987). This power law dependence has recently been observed in spectra of horizontal kinetic energy (Conway et al., 2019; Hertzog & Vial, 2001; Hertzog et al., 2002; Podglajen et al., 2016; Schoeberl et al., 2017); potential energy (Podglajen et al., 2016; Schoeberl et al., 2017); and pressure, zonal winds, and meridional winds (Conway et al., 2019). Podglajen et al. (2016) found that the slope is steeper around the tropics than over Antarctica, which suggests a latitudinal dependence of the spectral slopes. While seasonality and latitudinal variability in GW flux has been reported in models and observations (e.g., Alexander et al., 2010; Geller et al., 2013), no investigations into the seasonal influence on GW intrinsic frequency spectral slopes have been conducted.

The power law dependence evident in spectral slopes of GW disturbances suggests that observations can be used to estimate GW amplitudes at frequencies too high to be observed or resolved in climate models. If the spectral slopes of GW disturbances are known as functions of latitude and season, observationally based high-frequency gravity wave (HFGW) parameterizations can be implemented in models. Examples of such empirical parameterizations used for the purpose of Lagrangian microphysics and chemistry modeling can be found in, for example, Podglajen et al. (2016) and Kärcher and Podglajen (2019). Information about GW spectral slopes is also useful to evaluate process-oriented GW parameterizations used to represent the drag exerted by GWs on the background flow in general circulation models (GCMs) (e.g., de la Cámara et al., 2014).

Here we use Loon SPB data from 2014 to 2018 (Candido, 2020) to investigate GW variability over the entire intrinsic frequency spectrum as functions of latitude and seasonality. We interpolate the observations to 60 s intervals and divide the flights into 2 day segments, thereby producing 6,811 individual segments capable of resolving GW motions of periods ranging from 1 to 720 cycles/day, spread over all seasons and latitudes outside of the polar regions. We calculate horizontal eddy kinetic energy ( $E_{kh}$ ), potential energy ( $E_p$ ), and vertical kinetic energy ( $E_{kv}$ ) spectra; the  $E_{kh}$  spectra are calculated separately for five different latitudinal regions and four seasons. We fit the  $E_{kh}$  spectra to a  $\hat{\omega}^\gamma$  power law in five different frequency windows (expressed in terms of oscillation periods): 12 hr to 10 min, 6 hr to 10 min, 4 hr to 19 min, 13 to 6 min, and 4 to 2 min. The first two frequency windows are chosen for two reasons: first, the values of  $\gamma$  are reasonably constant in these windows, and second, spectral slope estimates in these frequency windows can be used to infer unresolved  $E_{kh}$  in GCMs from the resolved part of the GW intrinsic frequency spectrum. Indeed, Podglajen

et al. (2020) have shown that European Centre for Medium-Range Weather Forecasts (ECMWF) operational analysis and ERA5 reanalysis have cutoffs in  $E_{kh}$  at about 4 cycles/day (6 hr oscillations) in intrinsic frequency in the tropics. The other three windows are chosen for comparison with the results obtained by Podglajen et al. (2016). Estimates of  $\gamma$  for the five latitudinal regions over the four seasons are obtained in all five frequency windows, and the statistical significance of slope differences is estimated. Finally, we investigate the connections between the phase of the quasi-biennial oscillation (QBO) and amplitudes of  $E_{kh}$ ,  $E_{kv}$ , and  $E_p$ , as well as the spectral slopes of  $E_{kh}$ . We show that GW amplitudes are higher during positive QBO phases compared to negative phases for frequencies up to about 200 cycles/day and that spectral slopes are slightly steeper during positive QBO phases. We discuss the implications of our results for GW parameterizations in climate models.

## 2. Methods

### 2.1. Data

We use observations from Loon SPBs active from April 2014 to December 2018. The SPBs record a number of parameters during their flights, and we make use of the latitude, longitude, pressure, meridional wind, and zonal wind output. The measurement errors are  $\pm 2.5$  m for position and  $\pm 1$  hPa for pressure (horizontal winds are calculated from position data measured by GPS). Data are sampled at 1 Hz on the balloon and downloaded at intervals ranging from 10 s to 20 min, with the most frequent interval being 60 s. The mean SPB pressure level is 72 hPa with a standard deviation of 17 hPa, and 5th and 95th percentiles of 52 and 104 hPa, respectively. There are 1,182 unique SPB flights in our data set, and 828 of these are over 2 days long. The spread in flight duration is large, with 122 flights lasting over 100 days and the longest one lasting 197 days.

### 2.2. Data Processing

We focus our attention on the 828 flights exceeding 2 days in length, since these flights can be used to obtain GW spectra of periods of 1 day and shorter. The data from these flights are extensively processed before analysis; the processing includes replacing missing or unrealistic (corrupted) measurements, knitting together the data stream temporally, and interpolating the data linearly onto a regular time grid. The knitting together of the data stream is necessary to obtain segments of sufficient length; however, the process creates a discontinuity in the tendency of the data stream which may introduce a bias in high-frequency measurements. Spectral amplitudes of periods shorter than 10–15 min should be interpreted with caution. The data processing is described in detail in Text S1 of the supporting information.

At the end of the data processing the 828 flights have been separated into 6,811 two-day segments containing horizontal wind and pressure measurements every 60 s. Of these 6,811 segments 4,490 contain reliable, high-frequency pressure measurements. For data with reliable pressure measurements the mean pressure level is 77 hPa with a standard deviation of 10 hPa, and 5th and 95th percentiles of 61 and 95 hPa, respectively. The corresponding numbers for all 6,811 segments are 71, 13, 52, and 93 hPa. Figure 1 shows the mean locations of the 2 day segments in these two categories and illustrates the wealth of measurements available in the data set. There is exceptional seasonal coverage in the tropics over the Americas and good longitudinal coverage between 20°S and 60°S when reliable pressure measurements are not needed (Figure 1a). Most of the segments with reliable pressure measurements are located in the tropics (Figure 1b).

### 2.3. Analysis

We calculate the power spectral densities (PSDs) of  $u$ ,  $v$ , and  $\zeta_\theta$  for each 2 day segment using a Morlet wavelet transform with  $\omega_0 = 6$  and  $\delta t = 60$  s (Torrence & Compo, 1998).  $u$  is zonal wind,  $v$  is meridional wind, and  $\zeta_\theta$  is the isentropic wave-induced vertical displacement. The vertical displacement is estimated as  $\alpha \zeta'_\theta = \zeta'_b$ , where  $\zeta'_b$  is the balloon displacement and  $\alpha$  is taken to be equal to 0.3 (Podglajen et al., 2014; Vincent & Hertzog, 2014).  $\zeta_b$  is calculated from log-pressure height using a scale height specific to each 2 day segment  $n$ , equal to  $H_n = RT_n/g$ .  $R$  is the gas constant for dry air,  $g$  is acceleration due to gravity, and  $T_n$  is the mean temperature over the duration of the segment, over the range of latitudes and longitudes covered, and interpolated to the mean pressure level of the segment.  $T_n$  is obtained from 8 times daily MERRA-2 reanalysis data (Gelaro et al., 2017).

To limit edge effects, the segments are padded with zeros before the wavelet transform; the zeros are removed afterward. A global mean over all local wavelet spectra is then taken (i.e., a mean of the spectra at each time

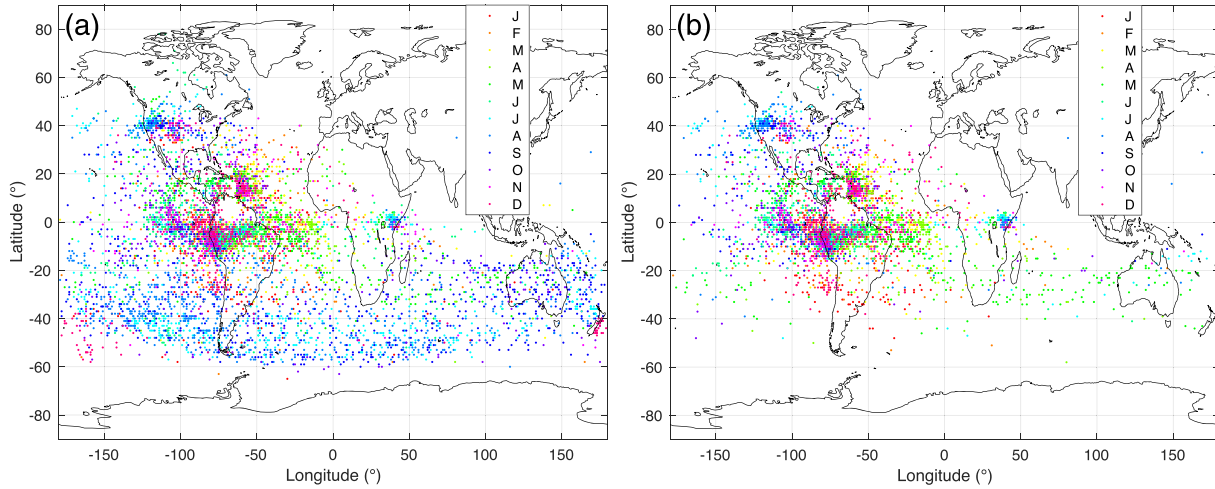


**Figure 1.** Distribution of (a) all 6,811 two-day segments and (b) the 4,490 two-day segments where reliable pressure measurements are available. The color coding shows the month of year for each individual segment.

step in the original time series). The signals at low frequencies and at local spectra close to the end points are attenuated due to edge effects, something that can be accounted for by calculating a cone of influence (COI) which shows where this attenuation becomes important. We have chosen not to do this: We are primarily interested in the amplitudes in the middle of the frequency spectra, and excluding 40% of the local spectra (the 20% closest to the end points in the beginning and end of the original time series; well outside any COI) has very limited impact on the global mean spectra (not shown). It is also worth noting that GWs are intermittent and that their amplitudes can vary strongly on time scales of a few wave periods (e.g., Hertzog et al., 2012; Plougonven et al., 2013); global means over all local wavelet spectra will therefore underestimate the amplitudes of individual wave packets. Although our study is not focused on GW intermittency, it should be noted that the statistical results of the spectra presented here hold despite this intermittency of the GW field. In particular, besides mean spectra in different conditions, we examine the dispersion of all 2 day average individual wavelet coefficients. The amplitudes obtained from global means provide useful constraints for HFGW parameterizations in GCMs, where mean wave activity is largely indicative of the influence on the overall circulation.

From our PSD calculations we know  $u'^2$ ,  $v'^2$ , and  $\zeta_\theta'^2$  as functions of intrinsic frequency ( $\hat{\omega}$ ). Following Podglajen et al. (2016), we calculate horizontal eddy kinetic energy ( $E_{kh}$ ), potential energy ( $E_p$ ), and vertical kinetic energy ( $E_{kv}$ ) for the segments to characterize GW variability. The quantities are defined as

$$E_{kh} = \frac{1}{2} (u'^2 + v'^2), \quad (1)$$

$$E_p = \frac{1}{2} N^2 \zeta_\theta'^2, \quad (2)$$

$$E_{kv} = \left( \frac{\hat{\omega}}{N} \right)^2 E_p. \quad (3)$$

The buoyancy frequency ( $N$ ) is calculated with MERRA-2 temperature data, and like in the case of  $T_n$ , a mean over the duration and horizontal extent is calculated and interpolated to the mean pressure level of the segment.  $E_{kh}$  is calculated for all 6,811 two-day segments, while  $E_p$  and  $E_{kv}$  are only calculated for the 4,490 segments with reliable pressure measurements.

The global wavelet spectrum of each segment provides estimates of GW amplitudes as a function of intrinsic frequency. The spectral slopes are fitted to a  $\hat{\omega}^\gamma$  power law through a linear fit in log-log space, in five different frequency windows (expressed throughout the manuscript in terms of oscillation periods): 12 hr to 10 min (12h-10m), 6 hr to 10 min (6h-10m), 4 hr to 19 min (4h-19m), 13 to 6 min (13m-6m), and 4 to 2 min (4m-2m). At periods shorter than about 10 min the slope is no longer linear in log-log space (see Figure 2),

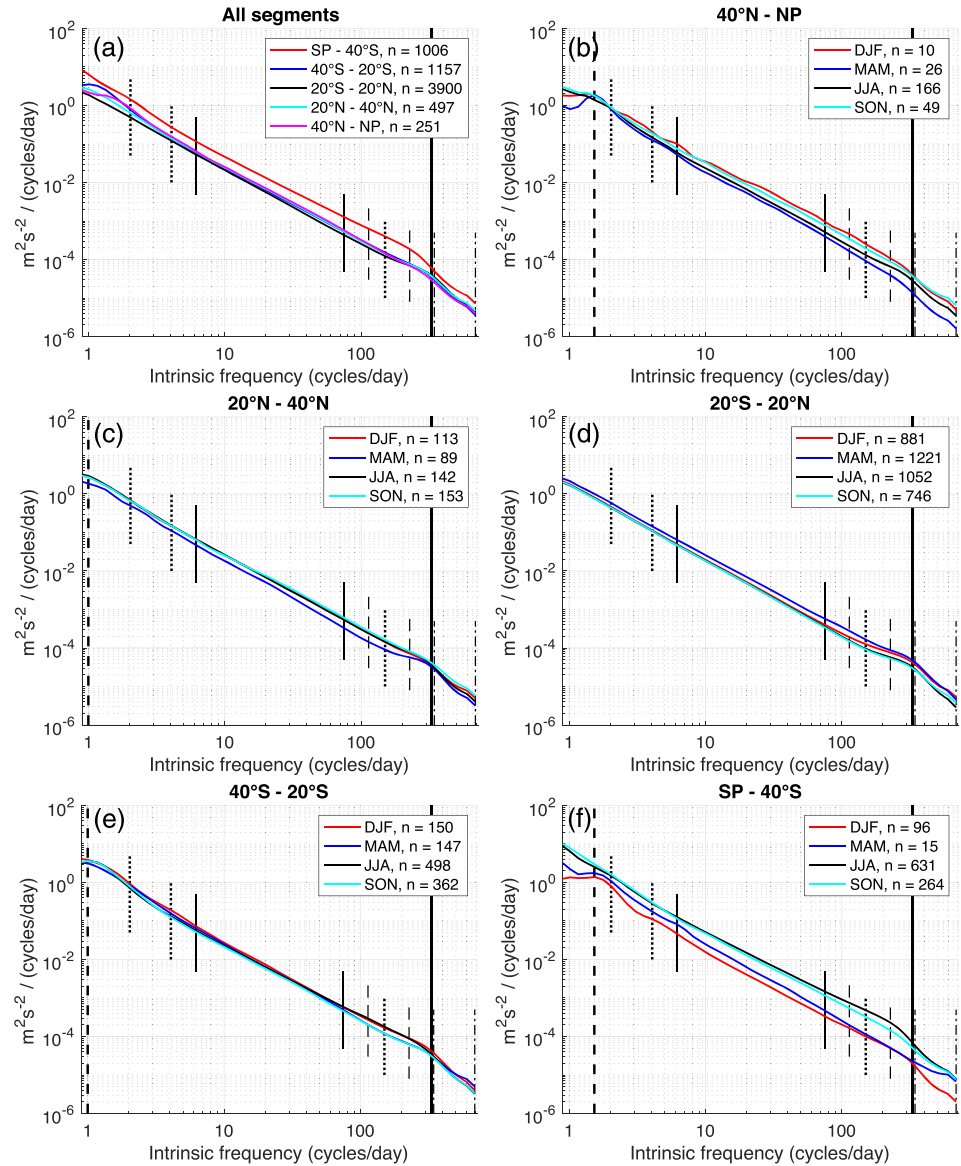


**Figure 2.** Amplitude spectra of  $E_{kh}$ , calculated for (a) five latitudinal regions without distinguishing seasons, and seasonal means for latitudes (b) 40°N to NP, (c) 20–40°N, (d) 20°S to 20°N, (e) 40–20°S, and (f) SP to 40°S. The number of 2 day segments in each category ( $n$ ) is displayed. The thick, vertical, solid lines mark a buoyancy frequency of  $N = 0.024 s^{-1}$ , while the thick, vertical, dashed lines mark Coriolis frequencies at 30° (c and e) or 50° (b and f). The thin, vertical lines mark frequencies between which slopes were estimated, with dotted lines marking oscillation periods of 12 hr, 6 hr, and 10 min; solid lines 4 hr and 19 min; dashed lines 13 and 6 min; and dot-dashed lines 4 and 2 min.

and this can be considered an upper frequency limit when inferring GW characteristics from low-frequency measurements. The 12h-10m and 6h-10m slopes largely obey a power law with constant  $\gamma$ , and by obtaining slope estimates in these frequency windows one can infer GW amplitudes at oscillation periods down to 10 min from measurements or models resolving GWs of intrinsic frequencies of 2 and 4 cycles/day. In other words, these slopes can be used to infer HFGW amplitudes from intrinsic frequencies resolved in typical reanalysis data (Podglajen et al., 2020).

The latter three windows are based on those found in Podglajen et al. (2016) and are included to facilitate comparisons with their results. The 4h-19m slopes are generally similar to those found for 12h-10m and 6h-10m, while the other two regions show slopes at frequencies just below  $N$  (13m-6m) and at frequencies just above  $N$  (4m-2m).



The segments are then separated by season and latitude to investigate the seasonality and latitudinal variability of GWs. In addition, we separate tropical spectra by QBO phase, where the QBO phases are determined from monthly zonal mean zonal winds at 30 hPa obtained from the National Oceanic and Atmospheric Administration (NOAA, 2020). Although the QBO phase is defined at a higher altitude than the mean balloon locations, the GW activity inferred from the balloons provide information about wave activity propagating upward into the stratosphere (Haynes et al., 1991). Means and standard deviations of the slopes are calculated for each subdivision, providing us with estimates of GW amplitudes and spectral slopes as a function of latitude, season, and, in the case of the tropics, QBO phase. The statistical significance of differences between the slopes of different regions, seasons, or QBO phases is estimated with a bootstrap resampling method that is described in detail in Text S2 of the supporting information. The results of the statistical significance tests are displayed in Table S2.

### 3. Results

#### 3.1. Horizontal Kinetic Energy Spectra

Figure 2 shows the spectral amplitudes of  $E_{kh}$  as functions of intrinsic frequency, sorted into five latitudinal regions and grouped by season. Thin, vertical lines mark the regions where spectral slopes have been fitted to a  $\omega^\gamma$  power law. The values of  $\gamma$ , along with the standard deviations of the fits, can be found in Tables 1 (for the 12h-10m, 6h-10m, and 4h-19m regions) and S1 (for the 13m-6m and 4m-2m regions). Table S2 shows the statistical significance of differences between the slopes.

Figure 2a displays the mean spectra of all measurements in the five latitudinal regions and shows that all regions except South Pole (SP) to 40°S have similar spectral amplitudes in the entire frequency range. It is important to note that the means of all measurements are not true annual means, since the seasonal sampling is not evenly distributed. The SP to 40°S region is particularly biased with 89% of the segments occurring during hemispheric winter and spring, where amplitudes are significantly higher than other months (see Figure 2f). The segments are more evenly distributed and the seasonal variability is lower in the other four regions.

The spectral slopes in the 12h-10m and 6h-10m windows are of greatest interest, since they can be used to infer GW amplitudes of periods down to 10 min from intrinsic frequencies resolved in reanalysis data (Podglajen et al., 2020). Slope fits in these regions generally vary little, with standard deviations for fits in different regions and seasons never exceeding 0.17 (see Table 1). When disregarding seasonal distributions, the 12h-10m slopes are all between  $\gamma = -1.96$  and  $\gamma = -1.94$ , except in the SP to 40°S region, where the slope is significantly shallower with  $\gamma = -1.86$ . The mean slope in the 12h-10m region over all latitudes and seasons is  $\gamma = -1.94$ , with a standard deviation of 0.14. The same latitudinal dependence can be seen in the 6h-10m window, with all slopes excluding the SP to 40°S region reaching values between  $\gamma = -1.95$  and  $\gamma = -1.92$ ; the slope in the SP to 40°S region is  $\gamma = -1.81$ . The mean slope in the 6h-10m region over all latitudes and seasons is  $\gamma = -1.92$ , with a standard deviation of 0.15.

The spectral slopes fitted over all seasons in the 4h-19m window are steepest in the tropics ( $\gamma = -1.96$ ), shallower in the extratropics, and shallowest furthest poleward ( $\gamma = -1.88$  and  $-1.81$  for north and south, respectively). That the slopes are steepest in the tropics and shallower poleward is in qualitative agreement with the measurements obtained by Podglajen et al. (2016) in this frequency window: They found slopes of  $\gamma = -1.96$  in the tropics and  $\gamma = -1.78$  in the polar region. The equatorial balloons used by Podglajen et al. (2016) were active between February and May, while the SH balloons flew between September and January. Taking seasonality into account (see below), comparable slopes from our balloons would be around  $-1.94$  and close to  $-1.9$  for the tropics and SH, respectively. An inverted latitudinal dependence is found in the 13m-6m window, where the slopes are shallowest in the tropics ( $\gamma = -1.5$ ) and steepest further poleward ( $\gamma = -2.0$  and  $-1.8$  for north and south, respectively). Podglajen et al. (2016) also found that the slopes in this region were shallow in the tropics ( $\gamma = -0.48$ ) and steeper in the SH polar region ( $\gamma = -1.58$ ), although their slopes were much shallower. The slopes in the 4m-2m window range between  $\gamma = -3.3$  and  $-2.9$ , with large standard deviations (up to 0.7). These slopes are also shallower than those found by Podglajen et al. (2016) in equivalent regions. Possible causes for the discrepancies in the slope estimates in these two windows of higher frequencies are addressed in section 4. The differences between most of the slopes in these three windows are statistically significant at a 95% significance level (see Table S2).

**Table 1**

Values of  $\gamma$  and Its Standard Deviation ( $\sigma$ ) for Fits in the 12h-10m, 6h-10m, and 4h-19m Windows as Functions of Latitudinal Region and Season

	12h-10m	6h-10m	4h-19m	Segments ( $n$ )
40°N to NP				251
DJF	$-1.87 \pm 0.15$	$-1.83 \pm 0.13$	$-1.78 \pm 0.14$	10
MAM	$-2.02 \pm 0.14$	$-1.98 \pm 0.13$	$-1.91 \pm 0.14$	26
JJA	$-1.96 \pm 0.13$	$-1.93 \pm 0.13$	$-1.89 \pm 0.15$	166
SON	$-1.91 \pm 0.11$	$-1.89 \pm 0.12$	$-1.84 \pm 0.13$	49
20–40°N				497
DJF	$-1.93 \pm 0.14$	$-1.92 \pm 0.14$	$-1.90 \pm 0.17$	113
MAM	$-1.99 \pm 0.10$	$-1.98 \pm 0.11$	$-1.98 \pm 0.15$	89
JJA	$-1.96 \pm 0.12$	$-1.94 \pm 0.12$	$-1.94 \pm 0.14$	142
SON	$-1.91 \pm 0.13$	$-1.90 \pm 0.15$	$-1.86 \pm 0.17$	153
20°S to 20°N				3,900
DJF	$-1.93 \pm 0.11$	$-1.93 \pm 0.12$	$-1.95 \pm 0.14$	881
MAM	$-1.93 \pm 0.13$	$-1.94 \pm 0.14$	$-1.94 \pm 0.17$	1,221
JJA	$-1.97 \pm 0.12$	$-1.97 \pm 0.13$	$-1.98 \pm 0.16$	1,052
SON	$-1.98 \pm 0.12$	$-1.98 \pm 0.13$	$-1.99 \pm 0.15$	746
QBO+	$-1.96 \pm 0.14$	$-1.97 \pm 0.15$	$-1.97 \pm 0.17$	1,820
QBO–	$-1.94 \pm 0.11$	$-1.94 \pm 0.12$	$-1.96 \pm 0.15$	2,080
40–20°S				1,157
DJF	$-1.98 \pm 0.12$	$-1.95 \pm 0.12$	$-1.95 \pm 0.15$	150
MAM	$-1.99 \pm 0.11$	$-1.96 \pm 0.11$	$-1.93 \pm 0.13$	147
JJA	$-1.91 \pm 0.16$	$-1.87 \pm 0.17$	$-1.87 \pm 0.19$	498
SON	$-2.00 \pm 0.14$	$-1.96 \pm 0.15$	$-1.95 \pm 0.19$	362
SP to 40°S				1,006
DJF	$-2.01 \pm 0.16$	$-1.97 \pm 0.17$	$-1.95 \pm 0.20$	96
MAM	$-2.03 \pm 0.13$	$-2.02 \pm 0.10$	$-1.99 \pm 0.11$	15
JJA	$-1.81 \pm 0.13$	$-1.76 \pm 0.12$	$-1.76 \pm 0.15$	631
SON	$-1.93 \pm 0.15$	$-1.87 \pm 0.13$	$-1.85 \pm 0.16$	264
All seasons				6,811
40°N to NP	$-1.96 \pm 0.13$	$-1.92 \pm 0.13$	$-1.88 \pm 0.14$	251
20–40°N	$-1.94 \pm 0.13$	$-1.93 \pm 0.14$	$-1.91 \pm 0.16$	497
20°S to 20°N	$-1.95 \pm 0.12$	$-1.95 \pm 0.13$	$-1.96 \pm 0.16$	3,900
40–20°S	$-1.95 \pm 0.15$	$-1.92 \pm 0.16$	$-1.91 \pm 0.18$	1,157
SP to 40°S	$-1.86 \pm 0.15$	$-1.81 \pm 0.15$	$-1.81 \pm 0.17$	1,006
All latitudes	$-1.94 \pm 0.14$	$-1.92 \pm 0.15$	$-1.92 \pm 0.17$	6,811

Note. The number ( $n$ ) of 2 day segments used for each fit can be found in the rightmost column. Divide  $\sigma$  by  $\sqrt{n}$  to obtain standard error of the mean.

The seasonality of GW amplitudes is evident when the segments are grouped by season and latitude (Figures 2b–2f and 3). There is little to no seasonality in the 20–40°N (Figure 2c), 20°S to 20°N (Figure 2d), and 40–20°S (Figure 2e) regions, but the amplitudes poleward of 40° (Figures 2b and 2f) are significantly higher during hemispheric winter. The weakest amplitudes in the Northern Hemisphere (Figures 2b and 2c) occur during spring (March–May, MAM), during the time of the stratospheric final warming (e.g., Butler et al., 2019). The seasonality is most pronounced in the SP to 40°S region (Figure 2f), where JJA (June–August) and SON (September–November) amplitudes are highest and DJF (December–February) amplitudes lowest. These results make sense intuitively, since the SH stratospheric final warming usually occurs in early November to late December (e.g., Haigh & Roscoe, 2009). Jewtoukoff et al. (2015) found

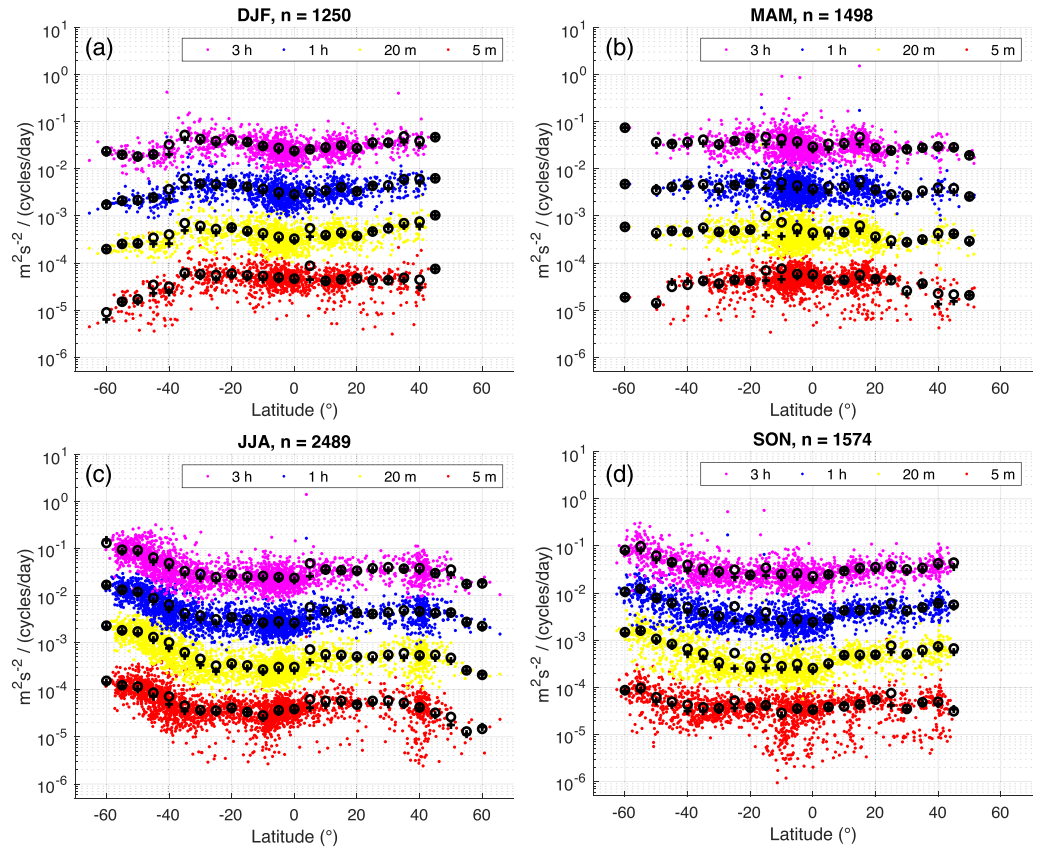


**Figure 3.**  $E_{kh}$  amplitudes for 3 hr, 1 hr, 20 min, and 5 min oscillations as a function of latitude, for (a) DJF, (b) MAM, (c) JJA, and (d) SON. Black circles (plus signs) show  $5^\circ$  latitude means (median values) for each period. The number of 2 day segments ( $n$ ) in each panel is shown.

that GW momentum flux in the SH polar region, measured both from SPBs and ECMWF operational analyses, decreased significantly from October to November and, in particular, December. Using the same SPBs and ECMWF analysis, as well as a mesoscale SH model, Plougonven et al. (2017) found a robust relationship between GW momentum fluxes and wind strength. They argued that their results were consistent with main GW sources being located in the tropospheric jet and lateral propagation of GWs into regions of strong winds. While these studies focused on GW momentum flux, one can expect that a similar dependence on wind strength should also be expected for other GW quantities, based on the polarization relations which relate perturbation amplitudes of different variables with one another (Fritts & Alexander, 2003). Since the zonal wind strength in the SH stratosphere is greatest during JJA and SON, and very weak immediately after the polar vortex collapse in DJF, the observed seasonality and latitudinal dependence in GW amplitudes may be partly explained by the relationship between GW variability and background wind magnitude.

Figure 3 shows scatter plots of spectral amplitudes at four different intrinsic frequencies as functions of season and latitude, and like Figure 2, it shows the seasonality of GW amplitudes at high latitudes (especially in the SH). However, Figure 3 also highlights the robustness of the latitude-amplitude relationship over a range of intrinsic frequencies: The fractional spread of amplitudes is similar for all oscillation periods, and the latitudinal variations follow the same patterns. Furthermore, Figure 3 includes  $5^\circ$  latitude mean and median values for the given intrinsic frequencies. Although the mean values tend to be higher than the median values, particularly where few data points exist, the mean and median values do not show strong latitudinal or seasonal discrepancies. This indicates that the observed seasonal and latitudinal variabilities are caused by mean shifts in GW amplitudes, rather than changes in the frequency of intermittent, high-amplitude GWs. The seasonal and latitudinal variations of  $E_{kh}$  amplitudes exhibit similar tendencies at all intrinsic frequencies and stand out of the internal variability in each season/latitude band. As a consequence, Figure 3 shows that good approximations of the latitudinal variability of HFGW amplitudes can be obtained from measurements at lower frequencies if the spectral slopes are known.



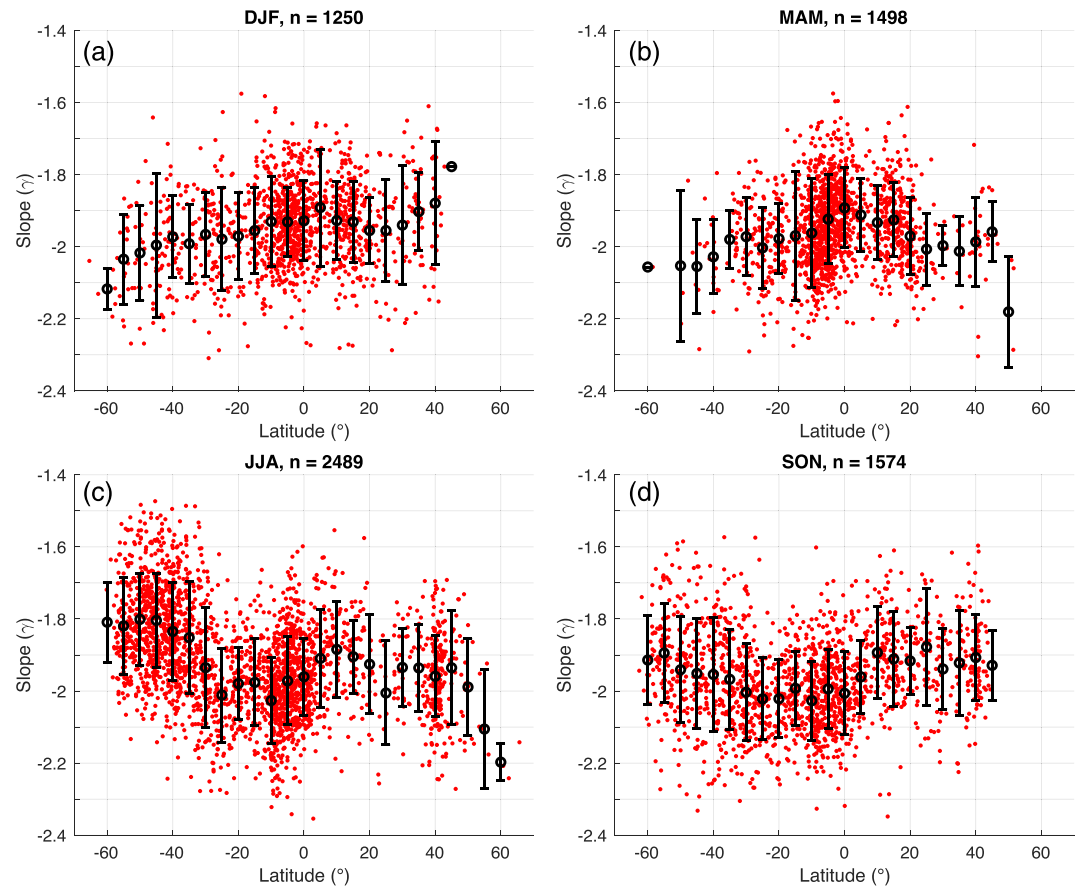


**Figure 4.** Spectral slopes (red dots) between oscillations of 12 hr and 10 min (leftmost and rightmost dotted lines in Figure 2) as a function of latitude, for (a) DJF, (b) MAM, (c) JJA, and (d) SON. Black circles and bars show 5° latitude means  $\pm 1$  standard deviation. The number of 2 day segments ( $n$ ) in each panel is shown. Outliers more than 3 standard deviations from the mean are excluded for display purposes.

In addition to the latitudinal variability mentioned above, the GW spectral slopes also exhibit some seasonal variability (Table 1). The slopes in the 12h-10m, 6h-10m, and 4h-19m windows show consistent seasonal variability close to the poles with shallower slopes during hemispheric winter: The JJA slopes are shallowest in the 20–40°S and SP to 40°S regions, while the DJF slopes are shallowest in the 40°N to NP (North Pole) region. The JJA and SON slopes in the SP to 40°S region are significantly shallower than their DJF and MAM counterparts; once again that is consistent with a SH final warming in late November or early December, thereby making SON winter-like in terms of stratospheric winds. The majority of the seasonal slopes in these windows are different from one another at a 95% confidence level, more so in the SH and the tropics than in the Northern Hemisphere, where observations are more sparse (see Table S2).

Scatter plots of 12h-10m spectral slopes as functions of latitude and season are shown in Figure 4. Slopes with magnitudes more than 3 standard deviations removed from the mean are not shown in the figure. The seasonality in the SH is evident. Spectral slopes for individual segments rarely deviate from the mean latitudinal values by more than about 0.3, and there is no clear latitudinal dependence on the spread of the slope values.

The seasonal spectral slopes in the 13m-6m and 4m-2m regions can be seen in Table S1. The standard deviations associated with the 13m-6m and 4m-2m slopes (around 0.5 and 0.7, respectively) are much larger than those in the 12h-10m, 6h-10m, and 4h-19m windows (none of which exceeds 0.20), and no consistent seasonal patterns can be seen. The shallowest 13m-6m slopes in both the 40°N to NP and SP to 40°S regions can be found in JJA, and the shallowest slope outside the tropics are during MAM in the 20–40°N region ( $\gamma = -1.4$ ). As mentioned previously, the slopes are generally shallowest in the tropics. Although the slopes

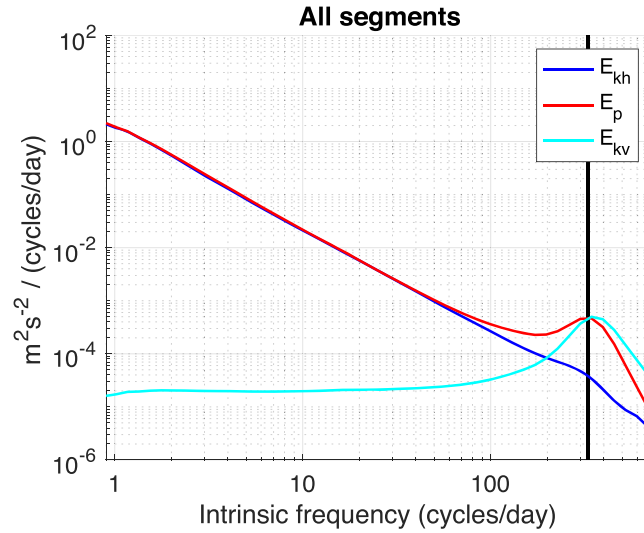


**Figure 5.** Mean amplitude spectra of  $E_{kh}$ ,  $E_p$ , and  $E_{kv}$  for all 4,490 segments containing reliable pressure measurements. The solid vertical line mark a buoyancy frequency of  $N = 0.024 \text{ s}^{-1}$ .

in the  $20^\circ\text{S}$  to  $20^\circ\text{N}$  region vary by season, this variability is likely due to the QBO rather than seasonality, since the slope differences between the individual seasons are smaller than those between positive and negative QBO phases. The role of the QBO in tropical GW spectra is discussed below.

### 3.2. Potential Energy Spectra

The spectra of  $E_{kh}$  and  $E_p$  should be similar to one another if the disturbances measured by the balloon are caused by GWs, through the GW polarization relations (Podglajen et al., 2016):

$$E_p = \left( \frac{N^2}{N^2 - \hat{\omega}^2} \right) \left( \frac{\hat{\omega}^2 - f^2}{\hat{\omega}^2 + f^2} \right) E_{kh}. \quad (4)$$

To check that the  $E_{kh}$  measurements are in fact associated with GWs, we calculate  $E_{kh}$ ,  $E_p$ , and  $E_{kv}$  from the segments that contain reliable pressure measurements. Seventy-nine percent of these segments are found in the tropics (see Figure 1b). The results are shown in Figure 5, which displays the mean  $E_{kh}$ ,  $E_p$ , and  $E_{kv}$  spectra for all 4,490 segments with reliable pressure measurements. The  $E_{kh}$  and  $E_p$  spectra are well matched up to frequencies of about 70 cycles/day (or periods around 20 min). Neutral, vertical balloon oscillations add to the  $E_p$  and  $E_{kv}$  spectra as the intrinsic frequency approaches that of  $N$ , and these spectra exhibit local maxima around the buoyancy frequency. Figure 5 shows that although log-log linearity extends down to periods as short as 10 min in  $E_{kh}$ , this type of behavior is only observed down to 20 min for  $E_p$ , in accord with previous campaigns (Podglajen et al., 2016).

### 3.3. Changes in Tropical Spectra Associated With the QBO

The QBO refers to the periodic reversals of zonal mean zonal wind observed in the equatorial lower stratosphere, something that occurs roughly every 28 months. The QBO dominates lower stratospheric wind variability in the tropics and has been shown to affect midlatitude circulation by altering the conditions for wave propagation into the stratosphere (Holton & Tan, 1980). The periodicity of the QBO comes from two-way interactions between propagating tropical waves and the mean flow: The phase speed of the waves and the strength and direction of the mean flow determine the propagation of the waves, while the momentum deposition of the waves at high altitudes affects and eventually reverses the direction of the mean flow (Plumb, 1984). The region of maximum wave convergence descends with time, thereby causing the wind reversal to migrate downward. When the equatorial wind at lower altitudes has reversed sign, waves of the opposite phase speed can propagate into the stratosphere, thereby starting the cycle again. The QBO is partially driven by GWs (e.g., Baldwin et al., 2001; Gray, 2013), and numerous studies have found correlations between the QBO phase and GW amplitudes (de la Torre et al., 2006; Ern et al., 2008; Krebsbach & Preusse, 2007; Wu & Eckermann, 2008) as well as GW momentum flux and drag (Ern et al., 2014) in satellite data. The wealth of measurements in our data set provides us with a unique opportunity to investigate GW spectral slopes and amplitudes at high frequencies during positive and negative phases of the QBO.

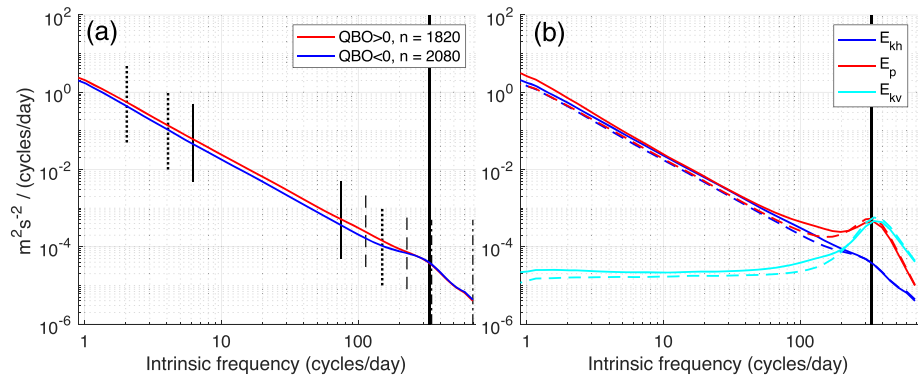


**Figure 6.** Amplitude spectra during positive (QBO > 0) and negative QBO (QBO < 0) phases in the 20°S to 20°N region. (a)  $E_{kh}$  for all 2 day segments, and (b)  $E_{kh}$ ,  $E_p$ , and  $E_{kv}$  for segments with reliable pressure measurements. The number of 2 day segments ( $n$ ) in each category is shown in panel a. Solid lines in panel b show positive QBO phases ( $n = 1,769$ ), while dashed lines show negative QBO phases ( $n = 1,767$ ). Vertical lines are equivalent to those in Figure 2. QBO phase is considered positive if monthly zonal mean zonal wind at the equator and 30 hPa is positive, and negative otherwise.

Figure 6 shows amplitude spectra in the 20°S to 20°N region separated by positive and negative phases of the QBO. The  $E_{kh}$ ,  $E_p$ , and  $E_{kv}$  amplitudes are higher for frequencies up to about 200 cycles/day during positive QBO phases compared to negative phases. The differences are highly statistically significant:  $t$  tests of slope differences between  $E_{kh}$  amplitudes at frequencies between 1 and 100 cycles/day give  $p$  values ranging from about  $10^{-4}$  to  $10^{-10}$ , depending on the frequency chosen.

During positive QBO phases the slopes in all five windows (Tables 1 and S1) are steeper than during negative QBO phases. These differences are statistically significant in all windows except the 4h-19m window. The slope differences are small (e.g.,  $\gamma = -1.96$  and  $\gamma = -1.94$  in 12h-10m window) with the exception of the 13m-6m window, where the slopes during positive and negative QBO phases are  $\gamma = -1.7$  and  $\gamma = -1.3$ , respectively. The slope in the 13m-6m window during negative QBO phases is shallower than any slope found when the segments in the region are separated by season only.

Although little seasonal variability is to be expected in the tropics, it is possible that seasonally biased sampling could affect the amplitudes and slopes attributed to the QBO. Figure 2d does show some seasonal variability in  $E_{kh}$  amplitudes, with slightly higher amplitudes during MAM and, to a smaller extent, DJF. However, it seems more likely that these differences are due to the QBO rather than actual seasonality. Figure S1 displays the number of segments during positive and negative QBO phases in the region by season and shows that most segments in DJF and MAM occur during positive QBO phases, while most segments in JJA and SON occur during negative QBO phases.

These results demonstrate a robust relationship between the QBO and GW activity in the lower stratosphere over two full QBO cycles. This relationship holds true for both vertical ( $E_p$  and  $E_{kv}$ ) and horizontal ( $E_{kh}$ ) GW motions and is persistent over a wide range of GW frequencies almost all the way up to that of the buoyancy frequency.

#### 4. Discussion

In this manuscript we have used Loon SPB data obtained from 2014 through 2018 to characterize GW variability over the entire intrinsic frequency spectrum in the lower stratosphere. The latitudinal and seasonal coverage provided by these balloons is unprecedented for such frequency ranges, and from these observations we have obtained some of the first seasonal and latitudinal estimates of GW variability at high frequencies. We use the observations to calculate slopes in  $E_{kh}$  spectra in five different frequency windows. Two of these windows (12h-10m and 6h-10m) can be used to extrapolate GW amplitudes to oscillation periods as short as 10 min from GWs resolved in current (re)analysis data sets (Podglajen et al., 2020). Since the slopes are calculated for different frequency windows and latitudinal regions, seasonally and latitudinally dependent extrapolations can be performed. This work therefore provides a concrete basis for estimating HFGW behavior over different seasons and latitudes.

The remaining three windows (4h-19m, 13m-6m, and 4m-2m) are included for comparison with results obtained from the SPB data analyzed by Podglajen et al. (2016). The 4h-19m window exhibits similar slopes, as well as seasonal and latitudinal variability, to the 12h-10m and 6h-10m windows, and our slope fits in the 4h-19m region are comparable to those obtained by Podglajen et al. (2016): We find mean slopes of  $-1.96 \pm 0.16$  in the tropics and  $-1.81 \pm 0.17$  for SP to  $40^\circ\text{S}$ , compared to the slopes of  $-1.96$  around the equator and  $-1.78$  poleward of  $60^\circ\text{S}$  obtained by Podglajen et al. (2016). The balloons used by Podglajen et al. (2016) were active between February and May (for equatorial flights) and September and January (SH flights). Taking seasonality into account, comparable slopes from our balloons would be around  $-1.94$  and close to  $-1.9$  for the tropics and SH, respectively. Note that Podglajen et al. (2016) did not provide standard deviations of the slope fits, only uncertainties in the fits of the mean slopes, so our standard deviations should not be compared to their estimated errors. Our slopes in the 13m-6m and 4m-2m regions are significantly different from those obtained by Podglajen et al. (2016), with Podglajen et al. (2016) finding shallower slopes between 12 and 6 min and steeper slopes between 4 and 2 min. We find no clear seasonality in these slopes, but a latitudinal dependence consistent with the results of Podglajen et al. (2016), with shallower (steeper) slopes in the tropics and steeper (shallower) slopes poleward for the 13m-6m (4m-2m) window. However, the standard deviations of these slopes are very large at about 0.5 and 0.7 for 13m-6m and 4m-2m, respectively. The discrepancies between our results and those of Podglajen et al. (2016) could be due to the different methods used to obtain GW spectra: Podglajen et al. (2016) used Fourier transforms to obtain their spectra, while we used wavelet transforms. The extensive processing of our data is another potential explanation, especially since the data processing disproportionately affects high-frequency measurements. Discrepancies due to differences in balloon or instrument design are also possible.

We showed that there is a strong seasonality in  $E_{\text{kh}}$  amplitudes close to the poles over a range of GW frequencies, with highest amplitudes during hemispheric winter. Although it is well documented that GW amplitudes have a strong seasonality close to the poles (e.g., Geller et al., 2013; Jewtougoff et al., 2015), our results demonstrate that this seasonal variability holds for the whole GW frequency range. Similarly, we show that spectral slopes in the 12h-10m, 6h-10m, and 4h-19m windows exhibit significant seasonality close to the poles, with shallower slopes during hemispheric winter. The seasonal differences, in terms of both amplitudes and slopes, are strongest in the SP to  $40^\circ\text{S}$  region. When spectral slopes are grouped by latitude over all seasons, the 12h-10m, 6h-10m, and 4h-19m slopes are steeper in the tropics and shallower closer to the poles (with the exception of the 12h-10m  $40^\circ\text{N}$  to NP slope). It is possible that this latitudinal dependence is underestimated in the  $40^\circ\text{N}$  to NP region, where the majority of measurements occur in summer (when slopes are steeper), and overestimated in the SP to  $40^\circ\text{S}$  region, where the majority of measurements occur in winter and spring (when slopes are shallower).

Furthermore, we estimated the variability in GW amplitudes and slopes in the  $20^\circ\text{S}$  to  $20^\circ\text{N}$  region with respect to the QBO. From over 3,500 two-day segments over two QBO cycles, we could show that  $E_{\text{kh}}$ ,  $E_{\text{kv}}$  and  $E_{\text{p}}$  amplitudes were higher during positive QBO phases compared to negative phases for frequencies up to about 200 cycles/day. The spectral slopes are steeper in all five frequency windows investigated, and the differences are statistically significant at a 95% confidence level in all windows except the 4h-19m window. These clear correlations between GW amplitudes and spectral slopes and the QBO phase highlight the importance of accurate GW parameterizations in climate models which aim to resolve the QBO. The scope of this study encompassed GW amplitudes and spectral slopes, but detailed interactions between GWs and the QBO need to be investigated by calculating GW drag under different QBO phases as well as vertical shears (e.g., Ern et al., 2014). Estimates of GW drag from Loon data is the subject of an ongoing study.

In this paper, we have focused on describing the mean wave activity as a function of intrinsic frequency. Although mean activity is the primary parameter for the forcing of the overall circulation and an important constraint for models, it has been shown that intermittent, large-amplitude waves can in some cases be the main contributors to overall GW momentum flux (e.g., Hertzog et al., 2012). Similar to scientific balloon data sets (e.g., Hertzog et al., 2012; Jewtougoff et al., 2015; Plougonven et al., 2013; Podglajen et al., 2020), the Loon data contains important information on GW intermittency which should be investigated in future studies.

In agreement with previous studies (e.g., Podglajen et al., 2016), we find that the spectra of  $E_{\text{kh}}$  and  $E_{\text{p}}$  were well matched up to frequencies around 70 cycles/day (20 min oscillations). At higher frequencies, close to the buoyancy frequency, neutral balloon oscillations affect the  $E_{\text{p}}$  and  $E_{\text{kv}}$  spectra. However, given the

similarities of  $E_p$  and  $E_{kh}$  spectra up to frequencies of 70 cycles/day, the spectral slopes can be used to infer  $E_p$  and  $E_{kv}$  amplitudes to intrinsic oscillation periods as low as 20 min.

Although Loon measurements cover large parts of the SH and tropics, the lack of measurements over Eurasia is a potential source of bias in estimates of Northern Hemisphere GW variability. It is likely that HFGWs have a strong longitudinal dependence in the Northern Hemisphere due to the presence of large-scale topography; this influence can be seen in measurements of GWs of larger scales and lower frequencies (e.g., Alexander et al., 2010; Geller et al., 2013). While much of the tropics are covered by Loon SPBs, there are very few observations over the Indian Ocean and western Pacific, which could be a source of bias in measurements of tropical GW variability.

The Loon data set is complementary to scientific balloon campaigns, which have the advantage of providing more reliable data (particularly at high frequencies), but lack the global coverage offered by Loon. Together, the two growing data sets will continue to provide a refined view of the intrinsic GW spectrum in the lower stratosphere in terms of both high-frequency waves and spatial and temporal variability of the spectrum, which will serve to improve parameterizations. Work using Loon measurements for producing physics-based HFGW parameterizations using ray-tracing and deep learning techniques is ongoing.

## Data Availability Statement

The data are publicly available and archived on Zenodo (Candido, 2020). MERRA-2 reanalysis data are available through NASA Goddard Earth Sciences Data and Information Services Center ([https://gmao.gsfc.nasa.gov/reanalysis/MERRA-2/data\\_access/](https://gmao.gsfc.nasa.gov/reanalysis/MERRA-2/data_access/)).

## Acknowledgments

Superpressure balloon data are provided by Loon LLC. The work was partly funded by the NSF through Grant AGS-1921409 to Stanford University. We thank Joan Alexander and Gilbert Compo for useful discussions.

## References

- Alexander, M. J., Bacmeister, J., Ern, M., Gisinger, S., Hoffmann, L., Holt, L., et al. (2019). Seeking new quantitative constraints on orographic gravity wave stress and drag to satisfy emerging needs in seasonal-to-subseasonal and climate prediction. *SPARC Newsletter*, 53, 31–36.
- Alexander, M. J., Geller, M., McLandress, C., Polavarapu, S., Preusse, P., Sassi, F., et al. (2010). Recent developments in gravity-wave effects in climate models and the global distribution of gravity-wave momentum flux from observations and models. *Quarterly Journal of the Royal Meteorological Society*, 136(650), 1103–1124. <https://doi.org/10.1002/qj.637>
- Alexander, S. P., Klekociuk, A. R., McDonald, A. J., & Pitts, M. C. (2013). Quantifying the role of orographic gravity waves on polar stratospheric cloud occurrence in the Antarctic and the Arctic. *Journal of Geophysical Research: Atmospheres*, 118, 11,493–11,507. <https://doi.org/10.1002/2013JD020122>
- Bacmeister, J. T., Eckermann, S. D., Newman, P. A., Lait, L., Chan, K. R., Loewenstein, M., et al. (1996). Stratospheric horizontal wavenumber spectra of winds, potential temperature, and atmospheric tracers observed by high-altitude aircraft. *Journal of Geophysical Research*, 101(D5), 9441–9470. <https://doi.org/10.1029/95JD03835>
- Baldwin, M. P., Gray, L. J., Dunkerton, T. J., Hamilton, K., Haynes, P. H., Randel, W. J., et al. (2001). The quasi-biennial oscillation. *Reviews of Geophysics*, 39(2), 179–229. <https://doi.org/10.1029/1999RG000073>
- Boccara, G., Hertzog, A., Basdevant, C., & Vial, F. (2008). Accuracy of NCEP/NCAR reanalyses and ECMWF analyses in the lower stratosphere over Antarctica in 2005. *Journal of Geophysical Research*, 113, D20115. <https://doi.org/10.1029/2008JD010116>
- Butler, A. H., Charlton-Perez, A., Domeisen, D. I. V., Simpson, I. R., & Sjöberg, J. (2019). Predictability of Northern Hemisphere final stratospheric warmings and their surface impacts. *Geophysical Research Letters*, 46, 10,578–10,588. <https://doi.org/10.1029/2019GL083346>
- Candido, S. (2020). Loon stratospheric sensor data. <https://doi.org/10.5281/zenodo.3763022>
- Conway, J. P., Bodeker, G. E., Waugh, D. W., Murphy, D. J., Cameron, C., & Lewis, J. (2019). Using Project Loon superpressure balloon observations to investigate the inertial peak in the intrinsic wind spectrum in the midlatitude stratosphere. *Journal of Geophysical Research: Atmospheres*, 124, 8594–8604. <https://doi.org/10.1029/2018JD030195>
- Coy, L., Schoeberl, M. R., Pawson, S., Candido, S., & Carver, R. W. (2019). Global assimilation of Loon stratospheric balloon observations. *Journal of Geophysical Research: Atmospheres*, 124, 3005–3019. <https://doi.org/10.1029/2018JD029673>
- de la Cámara, A., Lott, F., & Hertzog, A. (2014). Intermittency in a stochastic parameterization of nonorographic gravity waves. *Journal of Geophysical Research: Atmospheres*, 119, 11,905–11,919. <https://doi.org/10.1002/2014JD022002>
- de la Cámara, A., Lott, F. A., Jewtoukoff, V. A., Plougonven, R., & Hertzog, A. (2016). On the gravity wave forcing during the southern stratospheric final warming in LMDZ. *Journal of the Atmospheric Sciences*, 73(8), 3213–3226.
- de la Torre, A., Schmidt, T., & Wickert, J. (2006). A global analysis of wave potential energy in the lower stratosphere derived from 5 years of GPS radio occultation data with CHAMP. *Geophysical Research Letters*, 33, L24809. <https://doi.org/10.1029/2006GL027696>
- Dewan, E. M. (1994). The saturated-cascade model for atmospheric gravity wave spectra, and the wavelength-period (W-P) relations. *Geophysical Research Letters*, 21(9), 817–820. <https://doi.org/10.1029/94GL00702>
- Dharmalingam, S., Plougonven, R., Hertzog, A., Podglajen, A., Rennie, M., Isaksen, I., & Kébir, S. (2019). Accuracy of balloon trajectory forecasts in the lower stratosphere. *Atmosphere*, 10(2), 102. <https://doi.org/10.3390/atmos10020102>
- Dinh, T., Podglajen, A., Hertzog, A., Legras, B., & Plougonven, R. (2016). Effect of gravity wave temperature fluctuations on homogeneous ice nucleation in the tropical tropopause layer. *Atmospheric Chemistry and Physics*, 16(1), 35–46. <https://doi.org/10.5194/acp-16-35-2016>
- Ern, M., Ploeger, F., Preusse, P., Gille, J. C., Gray, L. J., Kalisch, S., et al. (2014). Interaction of gravity waves with the QBO: A satellite perspective. *Journal of Geophysical Research: Atmospheres*, 119, 2329–2355. <https://doi.org/10.1002/2013JD020731>
- Ern, M., Preusse, P., Krebsbach, M., Mlynarczyk, M. G., & Russell III, J. M. (2008). Equatorial wave analysis from SABER and ECMWF temperatures. *Atmospheric Chemistry and Physics*, 8(4), 845–869. <https://doi.org/10.5194/acp-8-845-2008>



- Friedrich, L. S., McDonald, A. J., Bodeker, G. E., Cooper, K. E., Lewis, J., & Paterson, A. J. (2017). A comparison of Loon balloon observations and stratospheric reanalysis products. *Atmospheric Chemistry and Physics*, 17(2), 855–866. <https://doi.org/10.5194/acp-17-855-2017>
- Fritts, D. C., & Alexander, M. J. (2003). Gravity wave dynamics and effects in the middle atmosphere. *Reviews of Geophysics*, 41(1), 3–1–3–64. <https://doi.org/10.1029/2001RG000106>
- Gary, B. L. (2006). Mesoscale temperature fluctuations in the stratosphere. *Atmospheric Chemistry and Physics*, 6(12), 4577–4589. <https://doi.org/10.5194/acp-6-4577-2006>
- Gelaro, R., McCarty, W., Suárez, M. J., Todling, R., Molod, A., Takacs, L., et al. (2017). The Modern-Era Retrospective Analysis for Research and Applications, Version 2 (MERRA-2). *Journal of Climate*, 30(14), 5419–5454. <https://doi.org/10.1175/JCLI-D-16-0758.1>
- Geller, M. A., Alexander, M. J., Love, P. T., Bacmeister, J., Ern, M., Hertzog, A., et al. (2013). A comparison between gravity wave momentum fluxes in observations and climate models. *Journal of Climate*, 26(17), 6383–6405. <https://doi.org/10.1175/JCLI-D-12-00545.1>
- Gray, L. J. (2013). Stratospheric equatorial dynamics. In Polvani, L. M., Sobel, A. H., & Waugh, D. W. (Eds.), *The stratosphere: Dynamics, transport, and chemistry* (pp. 93–107): American Geophysical Union (AGU). <https://doi.org/10.1002/9781118666630.ch5>
- Haigh, J. D., & Roscoe, H. K. (2009). The final warming date of the Antarctic polar vortex and influences on its interannual variability. *Journal of Climate*, 22(22), 5809–5819. <https://doi.org/10.1175/2009JCLI2865.1>
- Haynes, P. H., McIntyre, M. E., Shepherd, T. G., Marks, C. J., & Shine, K. P. (1991). On the “downward control” of extratropical diabatic circulations by eddy-induced mean zonal forces. *Journal of the Atmospheric Sciences*, 48(4), 651–678. [https://doi.org/10.1175/1520-0469\(1991\)048<0651:OTCOED>2.0.CO;2](https://doi.org/10.1175/1520-0469(1991)048<0651:OTCOED>2.0.CO;2)
- Hertzog, A., Alexander, M. J., & Plougonven, R. (2012). On the intermittency of gravity wave momentum flux in the stratosphere. *JAS*, 69(11), 3433–3448. <https://doi.org/10.1175/JAS-D-12-09.1>
- Hertzog, A., Boccara, G., Vincent, R. A., Vial, F. A., & Cocquerez, P. (2008). Estimation of gravity wave momentum flux and phase speeds from quasi-Lagrangian stratospheric balloon flights. Part II: Results from the Vorcore campaign in Antarctica. *Journal of the Atmospheric Sciences*, 65(10), 3056–3070. <https://doi.org/10.1175/2008JAS2710.1>
- Hertzog, A., Cocquerez, P., Guilbon, R. A., Valdivia, J.-N. A., Venel, S. A., Basdevant, C., et al. (2007). Stratéole/Vorcore-long-duration, superpressure balloons to study the Antarctic lower stratosphere during the 2005 winter. *Journal of Atmospheric and Oceanic Technology*, 24(12), 2048–2061. <https://doi.org/10.1175/2007JTECHA948.1>
- Hertzog, A., & Vial, F. (2001). A study of the dynamics of the equatorial lower stratosphere by use of ultra-long-duration balloons: 2. Gravity waves. *Journal of Geophysical Research*, 106(D19), 22,745–22,761. <https://doi.org/10.1029/2000JD000242>
- Hertzog, A., Vial, F., Mechoso, C. R., Basdevant, C., & Cocquerez, P. (2002). Quasi-Lagrangian measurements in the lower stratosphere reveal an energy peak associated with near-inertial waves. *Geophysical Research Letters*, 29(8), 70–1–70–4. <https://doi.org/10.1029/2001GL014083>
- Hoffmann, L., Spang, R., Orr, A., Alexander, M. J., Holt, L. A., & Stein, O. (2017). A decadal satellite record of gravity wave activity in the lower stratosphere to study polar stratospheric cloud formation. *Atmospheric Chemistry and Physics*, 17(4), 2901–2920. <https://doi.org/10.5194/acp-17-2901-2017>
- Holton, J. R., & Tan, H.-C. (1980). The influence of the equatorial Quasi-Biennial Oscillation on the global circulation at 50 mb. *Journal of the Atmospheric Sciences*, 37(10), 2200–2208. [https://doi.org/10.1175/1520-0469\(1980\)037<2200:TIOTEQ>2.0.CO;2](https://doi.org/10.1175/1520-0469(1980)037<2200:TIOTEQ>2.0.CO;2)
- Jensen, E. J., Ueyama, R., Pfister, L., Bui, T. V., Alexander, M. J., Podglajen, A. A., et al. (2016). High-frequency gravity waves and homogeneous ice nucleation in tropical tropopause layer cirrus. *Geophysical Research Letters*, 43, 6629–6635. <https://doi.org/10.1002/2016GL069426>
- Jewtoukoff, V. A., Hertzog, A., Plougonven, R., Cámara, A., & Lott, F. A. (2015). Comparison of gravity waves in the Southern Hemisphere derived from balloon observations and the ECMWF analyses. *Journal of the Atmospheric Sciences*, 72(9), 3449–3468. <https://doi.org/10.1175/JAS-D-14-0324.1>
- Kärcher, B., & Podglajen, A. (2019). A stochastic representation of temperature fluctuations induced by mesoscale gravity waves. *Journal of Geophysical Research: Atmospheres*, 124, 11,506–11,529. <https://doi.org/10.1029/2019JD030680>
- Karpechko, A. Y., & Manzini, E. (2012). Stratospheric influence on tropospheric climate change in the Northern Hemisphere. *Journal of Geophysical Research*, 117, D05133. <https://doi.org/10.1029/2011JD017036>
- Krebsbach, M., & Preusse, P. (2007). Spectral analysis of gravity wave activity in SABER temperature data. *Geophysical Research Letters*, 34, L03814. <https://doi.org/10.1029/2006GL028040>
- McDonald, A. J., & Hertzog, A. (2008). Comparison of stratospheric measurements made by CHAMP radio occultation and Stratéole/Vorcore in situ data. *Geophysical Research Letters*, 35, L11805. <https://doi.org/10.1029/2008GL033338>
- NOAA (2020). ESRL physical sciences division. Climate indices: Monthly atmospheric and ocean time-series.
- Pavelin, E., Whiteway, J. A., Busen, R., & Hacker, J. A. (2002). Airborne observations of turbulence, mixing, and gravity waves in the tropopause region. *Journal of Geophysical Research*, 107(D10), ACL 8–1–ACL 8–6. <https://doi.org/10.1029/2001JD000775>
- Plougonven, R., Hertzog, A., & Guez, L. (2013). Gravity waves over Antarctica and the Southern Ocean: Consistent momentum fluxes in mesoscale simulations and stratospheric balloon observations. *Quarterly Journal of the Royal Meteorological Society*, 139(670), 101–118. <https://doi.org/10.1002/qj.1965>
- Plougonven, R., Jewtoukoff, V. A., Cámara, A., Lott, F. A., & Hertzog, A. (2017). On the relation between gravity waves and wind speed in the lower stratosphere over the Southern Ocean. *Journal of the Atmospheric Sciences*, 74(4), 1075–1093. <https://doi.org/10.1175/JAS-D-16-0096.1>
- Plumb, R. A. (1984). The Quasi-Biennial Oscillation. In Holton, J. R., & Matsuno, T. (Eds.), *Dynamics of the middle atmosphere* (pp. 217–251): Terra Sci., Tokyo.
- Podglajen, A. A., Bui, T. P., Dean-Day, J. M., Pfister, L., Jensen, E. J., Alexander, M. J., et al. (2017). Small-scale wind fluctuations in the tropical tropopause layer from aircraft measurements: Occurrence, nature, and impact on vertical mixing. *Journal of the Atmospheric Sciences*, 74(11), 3847–3869. <https://doi.org/10.1175/JAS-D-17-0010.1>
- Podglajen, A. A., Hertzog, A., Plougonven, R., & Legras, B. (2016). Lagrangian temperature and vertical velocity fluctuations due to gravity waves in the lower stratosphere. *Geophysical Research Letters*, 43, 3543–3553. <https://doi.org/10.1002/2016GL068148>
- Podglajen, A., Hertzog, A., Plougonven, R., & Legras, B. (2020). Lagrangian gravity wave spectra in the lower stratosphere of current (re)analyses. *Atmospheric Chemistry and Physics Discussions*, 2020, 1–31. <https://doi.org/10.5194/acp-2020-7>
- Podglajen, A. A., Hertzog, A., Plougonven, R., & Žagar, N. (2014). Assessment of the accuracy of (re)analyses in the equatorial lower stratosphere. *Journal of Geophysical Research: Atmospheres*, 119, 11,166–11,188. <https://doi.org/10.1002/2014JD021849>
- Podglajen, A., Plougonven, R., Hertzog, A., & Jensen, E. (2018). Impact of gravity waves on the motion and distribution of atmospheric ice particles. *Atmospheric Chemistry and Physics*, 18(14), 10,799–10,823. <https://doi.org/10.5194/acp-18-10799-2018>

- Polichtchouk, I., Shepherd, T. G., & Byrne, N. J. (2018). Impact of parametrized nonorographic gravity wave drag on stratosphere-troposphere coupling in the Northern and Southern Hemispheres. *Geophysical Research Letters*, 45, 8612–8618. <https://doi.org/10.1029/2018GL078981>
- Pommereau, J.-P., Garnier, A., Held, G., Gomes, A. M., Goutail, F., Durry, G., et al. (2011). An overview of the HIBISCUS campaign. *Atmospheric Chemistry and Physics*, 11(5), 2309–2339.
- Pommereau, J.-P., Garnier, A., Knudsen, B. M., Letrenne, G. A., Durand, M., Nunes-Pinharanda, M., et al. (2002). Accuracy of analyzed stratospheric temperatures in the winter Arctic vortex from infrared Montgolfier long-duration balloon flights 1. measurements. *Journal of Geophysical Research*, 107(D20), SOL 2–1–SOL 2–18. <https://doi.org/10.1029/2001JD001379>
- Rabier, F., Cohn, S., Cocquerez, P., Hertzog, A., Avallone, L., Deshler, T., et al. (2013). The Concordiasi field experiment over Antarctica: First results from innovative atmospheric measurements. *Bulletin of the American Meteorological Society*, 94(3), ES17–ES20. <https://doi.org/10.1175/BAMS-D-12-00005.1>
- Schoeberl, M. R., Jensen, E., Podglajen, A., Coy, L., Lodha, C., Candido, S., & Carver, R. (2017). Gravity wave spectra in the lower stratosphere diagnosed from Project Loon balloon trajectories. *Journal of Geophysical Research: Atmospheres*, 122, 8517–8524. <https://doi.org/10.1002/2017JD026471>
- Sigmond, M., & Scinocca, J. F. (2010). The influence of the basic state on the Northern Hemisphere circulation response to climate change. *Journal of Climate*, 23(6), 1434–1446. <https://doi.org/10.1175/2009JCLI3167.1>
- Smith, S. A., Fritts, D. C., & Vanzandt, T. E. (1987). Evidence for a saturated spectrum of atmospheric gravity waves. *Journal of the Atmospheric Sciences*, 44(10), 1404–1410. [https://doi.org/10.1175/1520-0469\(1987\)044<1404:EFASSO>2.0.CO;2](https://doi.org/10.1175/1520-0469(1987)044<1404:EFASSO>2.0.CO;2)
- Spichtinger, P., & Krämer, M. (2013). Tropical tropopause ice clouds: A dynamic approach to the mystery of low crystal numbers. *Atmospheric Chemistry and Physics*, 13(19), 9801–9818. <https://doi.org/10.5194/acp-13-9801-2013>
- Torrence, C., & Compo, G. P. (1998). A practical guide to wavelet analysis. *Bulletin of the American Meteorological Society*, 79(1), 61–78. [https://doi.org/10.1175/1520-0477\(1998\)079<0061:APGTWA>2.0.CO;2](https://doi.org/10.1175/1520-0477(1998)079<0061:APGTWA>2.0.CO;2)
- van Niekerk, A., Sandu, I., & Vosper, S. B. (2018). The circulation response to resolved versus parametrized orographic drag over complex mountain terrains. *Journal of Advances in Modeling Earth Systems*, 10, 2527–2547. <https://doi.org/10.1029/2018MS001417>
- Vincent, R. A., & Hertzog, A. (2014). The response of superpressure balloons to gravity wave motions. *Atmospheric Measurement Techniques*, 7(4), 1043–1055. <https://doi.org/10.5194/amt-7-1043-2014>
- Wu, D. L., & Eckermann, S. D. (2008). Global gravity wave variances from Aura MLS: Characteristics and interpretation. *JAS*, 65(12), 3695–3718.